

# The influence of resolution and topographic uncertainty on melt modelling using hypsometric sub-grid parameterization

Felix Hebel\* and Ross S. Purves

*Department of Geography, University of Zurich, Winterthurer Str. 190, 8057 Zurich, Switzerland*

## Abstract:

Modelling of physical processes such as ablation or runoff at continental or global scales provides a key challenge: a high degree of abstraction is required in order to minimize computational demands, while spatial and temporal variability of key processes, often at the sub-scale level, need to be adequately captured and reproduced within a lower resolution model. For some approaches, such as temperature index models, downscaling to lower resolutions is straightforward. However a key issue when using these downscaled models is to assess the impact of scaling on model behaviour and results, including the associated uncertainties. We assess the impact of scaling on both a simple and an enhanced temperature index melt model from 100 m to 1, 5 and 10 km resolutions. Different sub-grid parameterization approaches are applied to both models across all resolutions and tested for their suitability against high-resolution reference data, with the aim of developing a robust, scalable and computationally undemanding parameterization. Results show patterns of over- and underestimation of potential melt rates for both models, with clear dependencies on scale, terrain roughness and variations of temperature thresholds, among other quantities. The sub-grid parameterizations tested in this article are found to effectively compensate these effects at little additional computational cost. Copyright © 2008 John Wiley & Sons, Ltd.

KEY WORDS melt modelling; sub-grids; parameterization; uncertainty; enhanced temperature index model; hypsometry

*Received 21 September 2007; Accepted 21 February 2008*

## INTRODUCTION

Models are a key tool in understanding and exploring of a wide variety of systems. Since all models, by definition, are an abstraction of reality, choosing an appropriate degree of abstraction is a key task. While complex processes need to be abstracted sufficiently so they can be understood and modelled, their key properties and dependencies must be retained. The scale and complexity of the processes to be modelled as well as the target range of scales over which a model should be applicable determines a target model resolution—however, in practice both the resolution and complexity of a model are often trade-offs between our ability to understand the system, the complexity of numerical solutions at a given resolution and computational capacities (e.g. Martin and Church, 2004; Armstrong and Martz, 2003; Malanson, 1999).

One example of this challenge lies in the modelling of ablation at global scales, which is increasingly important in estimating future water resources and, for example, in deriving boundary conditions for models of the behaviour of large ice sheets. Many present day ice sheets have very narrow ablation zones in terms of typical ice sheet model resolutions and overall ice sheet extents—for instance in Greenland the ablation zone has a width of around 20–60 km in comparison to a total ice sheet

width of approximately 800–1200 km and typical model resolutions of the order of 5–10 km (Alley *et al.*, 2005; Ritz *et al.*, 1997; Huybrechts *et al.*, 1996, 1991).

A promising approach to meeting the challenge of matching models and processes of differing scales lies in the application of so-called sub-grid approaches. Sub-grid approaches involve the parameterization of properties or processes that are not resolved at the grid scale. Other methods of coping with this problem include coupled and nested modelling (e.g. Salzmann *et al.*, 2007). Sub-grid modelling is characterized by storing additional layers of information on one variable while retaining the original model resolution. In geomorphological modelling, the use of hypsometric information (Strasser and Etchevers, 2003; Marshall, 2002; Marshall and Clarke, 1999) is a common approach. Rather than using one value of elevation for each model grid cell, attributes describing the hypsometry within each cell are also stored. This requires additional attributes per model cell, and attributes are most often stored in parallel grids. Sub-grid approaches can approximate information from much higher resolutions with relatively low additional computational costs for processing and storage.

If a new method of representing processes is developed, it must not only provide a means of resolving the process appropriately, its results should also be robust to uncertainty in its input parameters. This means that the inherent variation due to uncertainty in the input data should not trigger threshold effects, such as bifurcation of the model results, systematic over- or underestimation, or large deviation of model results for small variance in

\* Correspondence to: Felix Hebel, Department of Geography, University of Zurich, Winterthurer Str. 190, 8057 Zurich, Switzerland.  
E-mail: felix.hebel@geo.uzh.ch

input data. Therefore in this article we investigate three central questions:

- How does scaling impact potential melt rates calculated using temperature index models of different complexity?
- How can sub-grid approaches be used to effectively capture the variability of melt at low resolutions in mountainous regions?
- How sensitive are such approaches to typical uncertainties in input parameters?

#### *Low resolution melt modelling*

Simple temperature index models (TIM) (see for a review Hock, 2003) are often used for melt calculation in low resolution models running at continental or global scales, such as the GLIMMER ice sheet model (Hagdorn *et al.*, 2006). TIMs parameterize the complex physical processes and feedbacks in melt modelling based on the observation that potential melt is related to the time a snow or ice mass is exposed to temperatures above 0°C and the energy available for melting during this time. The potential melt energy is usually expressed as positive degree days (PDD). Melt is then calculated using a degree-day factor (DDF) which relates the temperature above 0°C to a melt rate.

TIMs have been shown to estimate melt rates well where reference melt data to calculate DDFs and temperature data are available (Braithwaite, 1995), and can be run using a minimum of computational resources. TIMs have been applied across a variety of temporal and spatial resolutions ranging from hours and 10s of metres to decades and 10s of kilometres. However, if reference melt or temperature data is inaccurate or of insufficient spatial density, TIMs can significantly over- or underestimate melt and fail to reproduce observed spatial variation.

To overcome these limitations, TIMs have been extended by a variety of authors to incorporate a radiation component (Pellicciotti *et al.*, 2005; Schneeberger *et al.*, 2003; Hock, 1999; Williams and Tarboton, 1999; Cazorzi and Fontana, 1996). Via calculation of solar radiation, these extended models explicitly incorporate topographic parameters such as slope and aspect, horizon- and self-shading, as well as time of year and latitude. While *de facto* no additional input parameters are needed, potential melt distribution can be modelled at a greater level of detail, both temporally and spatially, at the cost of additional computational demands. However, calculation times as well as data requirements are low compared to those of full scale energy balance models, which is why enhanced TIMs are often favoured, especially when modelling over extended spatial and/or temporal domains.

#### *Resolution effects and uncertainty*

Where TIMs are used in low resolution models, the input topography usually has to be re-sampled, from resolutions typically in the range of 100 m to 1 km (e.g. SRTM or Global Land One-kilometre Base Elevation

digital elevation models (GLOBE DEMs), Jarvis *et al.*, 2006; Hastings and Dunbar, 1998) to resolutions as low as 5, 10 or even 20 km. The smoothing effect this re-sampling has on topography and consequently on any associated parameter has been widely noted and the subject of a number of experiments, ranging from calculation of derivatives (Florinsky, 1998; Zhang *et al.*, 1999) to effects on spatial variability of parameters (Hu and Islam, 1997) and automatic analysis for environmental modelling (Albani *et al.*, 2004). In hydrology, effects of scale and consequently methods to minimize these effects have been explored, for example by Armstrong and Martz (2003). The use of elevation bands and sub-grids are common approaches to preserving crucial DEM information across resolutions in hydrological and related modelling (Luce *et al.*, 1999; Leung *et al.*, 1996). However, scaling and parameterization can have significant impacts on model behaviour and results. In order to improve the parameterization or assess the uncertainty associated with the model results, it is important to qualify and quantify these impacts (Wechsler, 2007; Hebeler and Purves, 2008a; Endreny and Wood, 2001).

#### *Aims*

The aims of this study are thus as follows:

- To investigate the effect of varying resolutions on absolute values as well as uncertainties of calculated potential melt rates using different melt models.
- To derive a method for melt calculation at low resolutions that:
  - delivers improved melt rates (when compared to reference data)
  - is scalable
  - is robust with low overall uncertainty
  - has low computational demands

## MATERIALS AND METHODS

For the experiments described in this article, potential melt for a study area is calculated using two models, namely a simple TIM and an enhanced temperature index model (eTIM), where an additional component models potential solar radiation. Potential melt is calculated at resolutions of 0.1, 1, 5 and 10 km and four sub-grid approaches using different parameterizations are compared. Figure 1 shows the schematic approach for calculating melt for each model, using different resolutions and parameterizations.

Additionally, to assess the robustness of the parameterization, the susceptibility of the different approaches to propagation of uncertainty in the input data is compared. Topographic uncertainty is simulated using a DEM uncertainty model, and its impact on calculated potential melt is explored using Monte Carlo simulation (MCS) (Hebeler and Purves, 2008a).

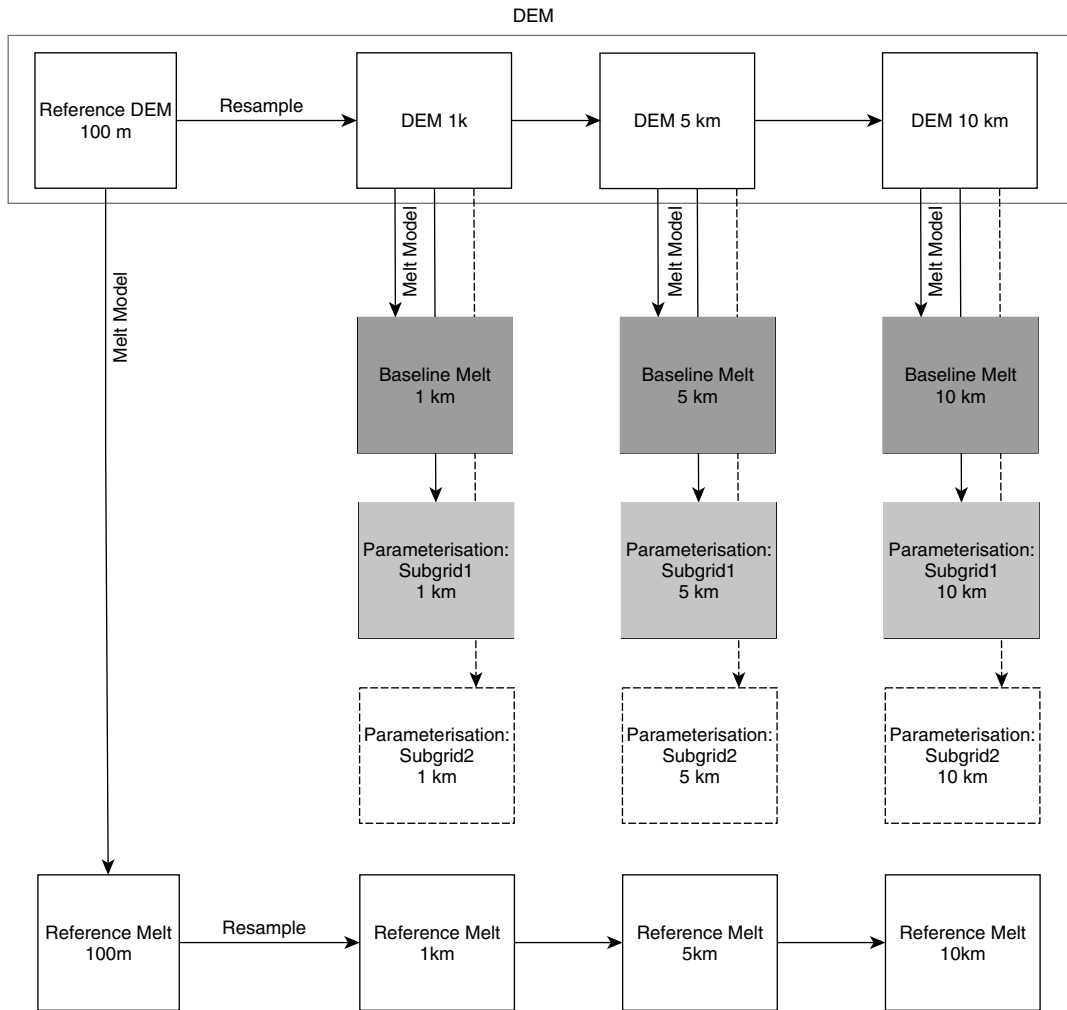


Figure 1. Experimental design: melt is calculated for resolutions of 100 m, 1, 5 and 10 km for both melt models following this scheme. At each resolution, a reference as well as an unparameterized baseline melt is calculated, and compared with alternative sub-grid parameterization approaches

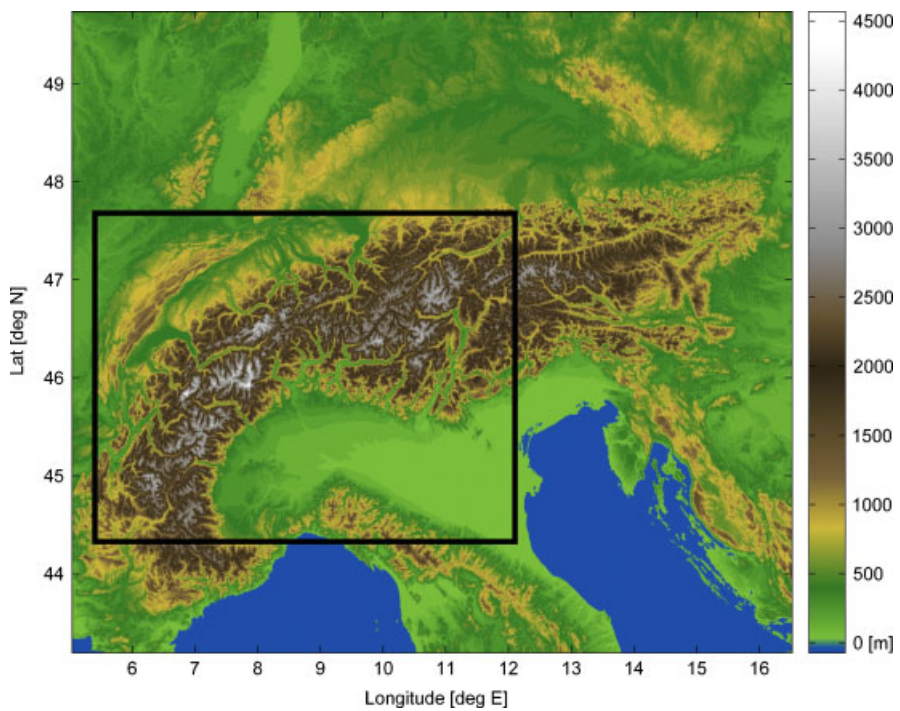


Figure 2. DEM of the European alps with the study area highlighted (solid black)

### Data

All model runs are conducted on a DEM of the European Alps (Figure 2). The study area lies between approximately 44 and 48°N latitude and 5 and 12°E longitude, with a total area of 201 000 km<sup>2</sup> and DEM altitudes ranging from sea level to 4654 m. All topography related calculations were conducted using hole-filled SRTM version 3 data at 3-arc-sec resolution (Jarvis *et al.*, 2006), projected to an Albers equal area projection at 100 m resolution using bilinear re-sampling.

For the sub-grid experiments, the original DEM was re-sampled to resolutions of 1, 5 and 10 km, where the re-sampled elevation value was derived from the mean of all the 100 m grid cells within the target resolution grid cell.

### Melt models

In our experiments, potential melt is calculated using a TIM and an enhanced version eTIM which includes the representation of potential solar radiation. Since a key aim of this work is to compare different sub-grid parameterization approaches for the TIM and eTIM, all model input parameters are assumed to be constant in time and space, with the exception of temperature and potential solar radiation. To avoid local effects and foster comparability, as well as limit the computational demands, a spatially constant mean annual air temperature at sea level was prescribed as input, and as a sinusoid with a period of 1 year and an amplitude of 5 °C. For each DEM grid cell, temperature is adjusted for elevation using a constant lapse rate of  $-6.5\text{ °C km}^{-1}$  (Stone and Carlson, 1979).

Furthermore, since we do not wish to reproduce particular mass balance or run-off scenarios, but are investigating potential melt, only a single DDF instead of separate DDFs for ice and snow is used. If we wished to reproduce real melt rates within a glacier or ice sheet model, then such assumptions are unrealistic, as many authors have shown that DDFs for ice and snow vary between and within catchments (e.g. Braithwaite, 1995).

**Temperature Index Model—TIM.** A number of authors have applied simple TIMs, which all follow the basic form given by Braithwaite (1995)

$$M_{\text{pot}} = \begin{cases} DDFT & T > T_t \\ 0 & T \leq T_t \end{cases} \quad (1)$$

where *DDF* is the degree day factor in  $\text{mm °C}^{-1} d^{-1}$  and *T* is the temperature in °C. Potential melt  $M_{\text{pot}}$  is set to zero for temperatures below a certain threshold temperature  $T_t$ , in our case 0 °C. Melt is calculated daily for each grid cell and integrated over 1 year.

**Enhanced Temperature Index Model—eTIM.** In order to enhance the TIM with a component representing potential solar radiation, the approach of Pellicciotti *et al.* (2005) is adopted, and the same temperature forcing as for the simple TIM is applied. In addition to the parameterizing melt using PDD and a degree-day melt factor, this

introduces a component that is directly dependent on potential direct shortwave radiation. Self- and horizon shading (Essery and Marks, 2007) are not considered in our model approach to minimize computation. Potential melt  $M_{\text{pot}}$  thus consists of a temperature term  $MT_{\text{pot}}$  and a radiation term  $MR_{\text{pot}}$

$$M_{\text{pot}} = MT_{\text{pot}} + MR_{\text{pot}} \quad (2)$$

and is derived as:

$$M_{\text{pot}} = \begin{cases} F_t \cdot T + F_r \cdot (1 - \alpha)R & T > T_t \\ 0 & T \leq T_t \end{cases} \quad (3)$$

where  $F_t$  is a temperature factor, *T* is the temperature,  $F_r$  is a radiation factor,  $\alpha$  is albedo, *R* is the shortwave radiation at the surface and  $T_t = 0\text{ °C}$  is the threshold temperature for melt to occur (Table I). Note that the temperature factor ( $F_t$ ) used in this equation is smaller than the commonly used DDFs (Pellicciotti *et al.*, 2005). In our experiments, the potential clear-sky direct solar radiation at the surface corrected for the incidence angle  $I_s$  in  $\text{Wm}^{-2}$  is calculated following Kumar *et al.* (1997):

$$I_s = S_0 \cdot \left( 1 + 0.0344 \cos \left( \frac{360^\circ d}{365} \right) \right) \tau_b \cos i \quad (4)$$

where  $d[1..365]$  is the day of the year,  $\tau_b$  is the atmospheric transmittance for beam radiation and *i* is the incident angle of the sun, which in turn is a function of the solar declination, slope and aspect. The total potential incoming solar radiation at the surface for each grid cell is then derived as follows:

$$R = I_s + I_d + I_r \quad (5)$$

where  $I_s$  is the potential direct radiation at the surface corrected for the incidence angle and atmospheric transmittance and  $I_d$  is the diffuse solar radiation, both calculated for clear-sky conditions.  $I_r$  is the radiation reflected from surrounding locations transmitted to the surface, calculated using a constant mean ground reflectance coefficient of 0.2, following Kumar *et al.* (1997).

Solar radiation *R* is calculated hourly for every grid cell and integrated over the calculated day length *dt*. Potential melt from solar radiation is then calculated according to Equation 3, using a relatively low, constant albedo of 0.4. While the albedos of snow, ice, debris and water range from 0.1 to 0.9 (Lefebvre *et al.*, 2003), a value of 0.4 attempts to represent the mean albedo over the area. At the same time, this low albedo ensures that potential melt from radiation is an important term in the eTIM model, providing a contrast with the TIM. Potential daily solar radiation is then converted to potential melt using  $F_t$  and added to potential daily melt derived using the daily mean temperature multiplied by the temperature factor  $F_t$ . As for the TIM, mean annual air temperature is varied over 1 year using a simple sinusoid function with an amplitude of 5 °C.

In this study, several simplifying assumptions have been made to facilitate computation and comparison of

results, a number of which have been disputed in the literature:

- Spatially invariant input parameters are used such as sea-level temperatures, DDFs, reflectance coefficient and albedo (compare e.g. Essery and Etchevers, 2004, Hock, 2003; Lefebre *et al.*, 2003).
- Potential melt is calculated using a single DDF, instead of ‘real’ ablation which would require a mass-balance (e.g. glacier) model and the use of separate DDFs for ice and snow (compare e.g. Hock, 2003; Braithwaite, 1995).
- A single mean albedo is used instead of different albedos for snow, ice, vegetated areas and barren ground (e.g. Pellicciotti *et al.*, 2005; Lefebre *et al.*, 2003), which again would necessitate a glacier model, the same holds for the reflectance coefficient.
- The threshold temperature for melt to occur is fixed at 0 °C, irrespective of the actual energy available for melt, which could cause this threshold to vary in time and space (e.g. Hock, 2005).
- Self- and horizon-shading is not considered in the radiation model, and conditions are assumed to be clear sky (e.g. Essery and Marks, 2007).

The cost of these simplifications inevitably is that any comparison with ‘real’ melt scenarios or observational data is not possible. However, in order to derive potential melt rates that lie within a realistic range, both melt models are tuned to approximately fit melt rates at selected locations reported by Strasser *et al.* (2004), by slightly adjusting the values for DDF and  $F_r$  used by Pellicciotti *et al.* (2005) for our case study. All adjusted parameters used in both models are given in Table I.

*Method comparison*

For each melt model at 1, 5 and 10 km resolution a *baseline* model run is performed without any sub-grid parameterization, that serves as a point of comparison. The aim of our sub-grid parameterizations is to give results close to the reference that mark an improvement over this baseline approach. All parameterized model runs are quantitatively compared with the baseline by calculating the root mean square error (RMSE) from

the reference and qualitatively explored to describe and discuss differences between the methods.

*Sub-grid parameterization*

The aim of sub-grid parameterization is to capture the spatial variability of the modelled process at its original resolution, while reducing the demands for data and computation by approximating the process at a lower resolution. In the simple TIM, melt is a function of temperature, which in turn is determined by elevation via the prescribed sea-level temperature and the lapse rate. Potential melt is thus a linear function of altitude for temperatures above 0 °C. Because temperature is varied over time, a ‘lower-threshold (LT altitude’, equivalent to the absolute frost line) exists, which separates areas with temperatures above 0 ° throughout the year, and areas where temperatures fall below zero for increasing time intervals during the year. As melt ceases during these intervals, the melt function becomes nonlinear for areas above LT. (Figure 3).

Potential melt calculated using the eTIM is influenced by temperature in a twofold manner: Firstly, the temperature dependent term of Equation 3 is equivalent to

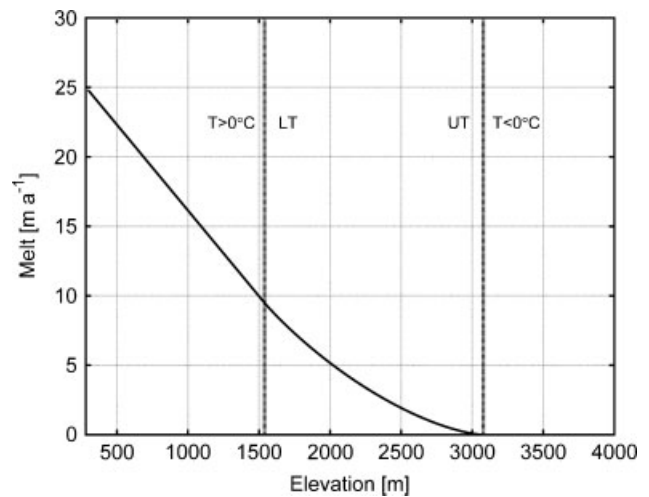


Figure 3. Potential melt as a function of altitude, calculated using the simple TIM over 1 year. Melt becomes nonlinear above a lower threshold (LT), the altitude above which temperature becomes 0 °C at least one day per year. Temperature is always below 0 for elevations above the upper threshold (UT)

Table I. Parameters used for the calculation of potential melt using the simple temperature index model and the enhanced solar radiation model

Symbol	Parameter	Value	Units
$\alpha$	Albedo	0.4	
$a_{seas}$	Seasonal temperature amplitude	5.0	°C
DDF	Degree day factor	5.2	mm d <sup>-1</sup> °C <sup>-1</sup>
$F_r$	Shortwave radiation factor	0.012	m <sup>2</sup> mm W <sup>-1</sup> h <sup>-1</sup>
$F_t$	Temperature factor	0.05	mm h <sup>-1</sup> °C <sup>-1</sup>
lrate	Atmospheric lapse rate	-6.5	°C km <sup>-1</sup>
MAAT	Mean annual air temperature at sea level	15.0	°C
$r$	Ground reflectance coefficient	0.2	
$S_0$	Solar constant	1367	W m <sup>-2</sup>
$T_t$	Temperature threshold for melt	0	°C

that of the TIM (Equation 1), and exhibits the same dependencies. Secondly, the radiation term is also influenced through temperature (Figure 4), because radiation incurred melt is also set to zero for days with temperatures below  $T_t$  (Pellicciotti *et al.*, 2005). Radiation melt can take on a range of values, for elevations below LT, as it is dependent on local slope and aspect. Because the atmospheric transmittance  $\tau_b$  (Equation 4) increases with elevation, radiation melt slowly increases towards LT. Analogous to temperature inferred melt, the radiation melt decreases with elevation above LT, because temperatures fall below zero for increasing intervals during the year, and melt ceases (Figure 4).

Since in our case, the radiation melt term contributes approximately 60% of the total melt, besides elevation (through its influence on temperature), any parameterization approach must also consider the factors of slope gradient and aspect that influence the spatial variability of radiation (Figure 5).

All sub-grid approaches presented within this article are based on hypsometric parameterization, which attempts to capture the variability of elevation within a given area. Because the aim of this work is to develop and test a method that is scalable, melt is calculated for resolutions of 1, 5 and 10 km. Sub-grid values are calculated for each of these resolutions by calculating the hypsometric curve based on the topography resolved at 100 m

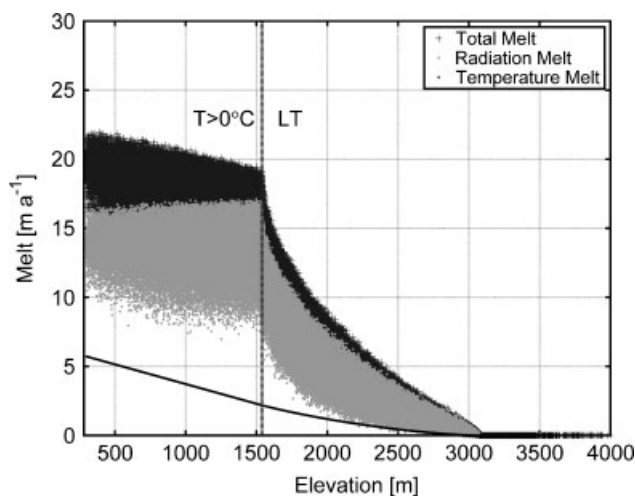


Figure 4. Potential melt plotted against elevation, calculated using the eTIM over 1 year. Below the 0 °C threshold (LT) melt values can take a range of values depending on slope and aspect. Radiation melt gradually increases with elevation (grey dots), while temperature melt (solid black line) decreases. For elevations above LT, potential radiation melt and thus total melt (dark grey +) decreases, because melt ceases for temperatures below 0 °C for increasing durations of the year

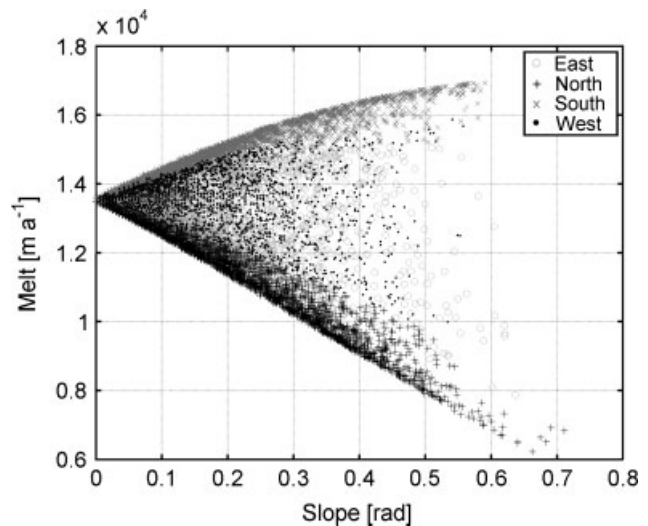


Figure 5. Potential melt from solar radiation versus slope per aspect quadrants (centred on the four cardinal directions). Melt calculated using the eTIM for elevations below the 0 °C threshold. Slope in radians. Melt increases with slope for south-facing slopes (grey x) and decreases for north-facing slopes (black +). The observable variation in calculated melt for a single slope value is caused by the variation of aspect within the respective 90° quadrant

within the respective low resolution cell. Three sub-grid layers are then created for each resolution, by storing the elevation values of the 0-15, 0-5 and 0-85 quantiles of the derived hypsometry for each cell. Thereby these sub-grids represent the mean altitude of the upper and lower 30% of elevation values and the median of all values. The thus derived elevation sub-grids are then used in all of the following parameterizations.

- **Sub-grid 1** Melt is calculated separately for each of the three elevation sub-grids, weighted according to the relative hypsometric area of each sub-grid (0-3, 0-4, 0-3) and summed. For the eTIM, slope and aspect are calculated directly on each sub-grid. Because for the eTIM slope is calculated within each elevation sub-grid, the full elevation range of topography is not honoured, and the slope might be biased. While for the TIM only three sub-grids are needed, technically nine sub-grids are used for the eTIM, as slope and aspect have to be calculated for each sub-grid (Table II).

Since the eTIM is dependent not only on elevation, but also on slope and aspect, sub-grid approaches that attempt to capture the variability of these parameters are introduced. These parameterizations are only applied to the eTIM, while sub-grid 1 is applied to both models:

Table II. Parameterization approaches used for the TIM and eTIM. All parameters/derivates not explicitly stated are calculated separately for every sub-grid

Name	Sub-grids	Description	Model
Sub-grid 1	3 (+3 + 3)	Elevation sub-grids (+ slope and aspect calculated on sub-grids for eTIM)	TIM and eTIM
Sub-grid 2	3 + 3 + 1	Elevation sub-grids + mean slope per elevation sub-grid + aspect	eTIM
Sub-grid 3	3 + 3 + 3	Elevation sub-grids + mean slope + mode of aspect per elevation sub-grid	eTIM
Sub-grid 4	5 + 4	Elevation sub-grids + mean slope per cardinal direction	eTIM

- Sub-grid 2** To avoid the biased calculation of slope within each sub-grid from the previous sub-grid 1 parameterization, for this approach slope is calculated at the reference resolution (100 m). Each cell is then classified into the elevation sub-grid class (either lower, median or upper third) to which they contribute at the low resolution (1, 5 or 10 km). The corresponding slopes are averaged for each of the sub-grids (Figure 6). While this requires one-time slope calculation at the highest resolution, slope is correctly calculated for each of the elevation sub-grids. Finally, one aspect value is calculated at the lower resolution for each cell. Thus, it is implicitly assumed that aspect values are more spatially auto-correlated and co-occur over larger areas, while the variation in slope is parameterized in the sub-grids. This gives a total of seven sub-grids for this approach (Table II).
- Sub-grid 3** For the third approach, slope is calculated for each elevation sub-grid class identical to sub-grid 2. Additionally, we attempt to capture the variation of aspect in sub-grids. Since aspect is a ‘circular’ variable, no average value can be derived. In our approach, aspect is calculated at the 100 m resolution and classified into 12 nominal classes [1..12], each covering 30°. Cells are again masked at the high resolution, similar to slope (Figure 6). The mode of the aspect classes within each sub-grid elevation class (upper/median/lower) is then assigned to the corresponding sub-grid. Thus, for each elevation sub-grid cell at the lower resolution,

aspect is determined by the aspect class of the majority of 100 m cells within each sub-grid elevation range.

- Sub-grid 4** In this approach, solar radiation is calculated using four sub-grids containing the average slope in the four quadrants centred on the cardinal directions (north, south, east and west) calculated at the 100 m resolution. For each sub-grid, maximum potential melt from radiation  $MR_{max}$  is calculated irrespective of the temperature condition in Equation 3 (assuming  $T$  always  $>T_i$ ), which delivers the maximum potential radiation melt, unreduced by temperature, over 1 year for the study area.

Additionally, five elevation sub-grids are used, adding the maximum and minimum elevation to the three previously used sub-grid elevations, giving a total of nine sub-grids for this approach (Table II). These values are then used to reduce maximum radiation melt for the amount influenced by temperature, by approximating the proportion of the area within each cell, which lies above the lower threshold (around 1500 m in Figure 4).

Potential radiation melt  $MR_{pot}$  (Equation 2) is thus calculated by reducing maximum radiation melt  $MR_{max}$  as follows:

$$MR_{pot} = MR_{max} - MR_{max}Q \tag{6}$$

The reduction factor  $Q$  is deduced using *reference* data calculated over 1 year at the 100 m resolution and re-sampled to the respective lower resolution of the sub-grids (compare Section 2.3). This (correctly reduced)

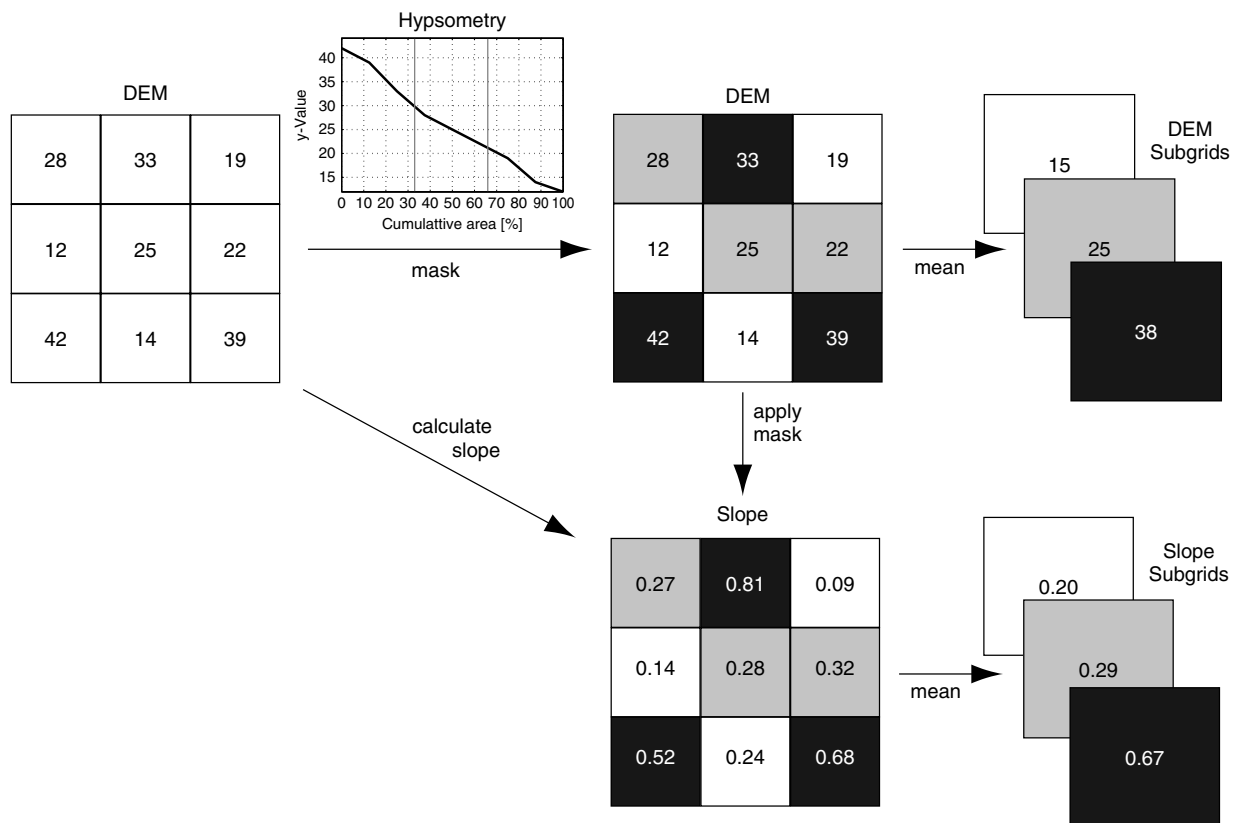


Figure 6. Scheme for calculating elevation and slope sub-grids (sub-grid 2): cells of the high-resolution DEM are masked according to the hypsometry class (upper/median/lower) they belong to at the respective lower resolution. DEM sub-grid values are directly derived using DEM quantiles, while slope is calculated per hypsometry class at the higher resolution

reference radiation melt  $MR_{ref}$  is then subtracted from the unreduced radiation melt  $MR_{max}$  for each cell to derive the reduction factor  $Q$  as

$$Q = \frac{MR_{max} - MR_{ref}}{MR_{max}} \quad (7)$$

$Q$  can be approximated using the following third order polynomial according to

$$Q = a_3 \cdot (t_{frac} + z_{frac})^3 + a_2 \cdot (t_{frac} + z_{frac})^2 + a_1 \cdot (t_{frac} + z_{frac}) + c \quad (8)$$

where  $t_{frac}[0..1]$  is the fraction of the DEM above the LT within each cell and  $z_{frac}[0..1]$  is the fraction of the DEM above the upper threshold (UT) (Figure 3).

A regression analysis to derive the terms of Equation 8 yielded similar results for the 5 and 10 km resolutions, with  $r^2$  values above 0.96, while parameters for the 1 km resolution were outside the 99% confidence interval of both the 5 and 10 km regression, also giving a distinctively lower fit ( $r^2 = 0.84$ ). Parameters used for the regression in our experiments were thus chosen from the 10 km resolution regression to be  $a_3 = 0.467$ ,  $a_2 = -1.031$ ,  $a_1 = -0.114$ ,  $c = -0.007$ . Without high-resolution reference, the fractions  $t_{frac}$  and  $z_{frac}$  have to be calculated using the five sub-grid elevations. As they have been calculated from the higher resolution hypsometry, the cumulative relative area for each sub-grid is known (0/0.15/0.5/0.85/1), and  $t_{frac}$  and  $z_{frac}$  can be approximated by linear interpolation between the cumulative area of the sub-grids below and above each threshold LT and UT.

Using  $t_{frac}$  and  $z_{frac}$  to calculate  $Q$ , the maximum radiation melt term  $MR_{max}$  can be corrected for temperature reduction to give  $MR_{pot}$  and added to the temperature melt term  $MT_{pot}$  (Equation 2), which is calculated similarly to the sub-grid 1 approach, using only the three original elevation sub-grids.

Table II summarizes the four sub-grid parameterization approaches and the total number of sub-grids required in each case.

#### Resolution experiments

Potential melt for both the TIM and eTIM is calculated in units of metres water equivalent per year (m w.e.  $a^{-1}$ ). A set of melt rates was calculated for each model at 100 m resolution, and then re-sampled to 1, 5 and 10 km resolution by averaging melt, thus conserving mass (Figure 1). This gives a **reference** melt distribution derived from the melt rates calculated at the 100 m resolution in m w.e.  $a^{-1}$  for each resolution and model. These sets allow comparison by serving as a reference for assessing the effect of scaling, and the fit of different parameterization approaches.

#### Uncertainty analysis

As stated in the introduction, the aim of this work is not solely to develop an effective parameterization that gives

improved results over the baseline approach, but also one that is robust towards uncertainty in the input data. Previous research (Hebeler and Purves, 2008a; Oksanen and Sarjakoski, 2005; Wechsler, 2000) has shown that sensitivity to DEM uncertainty is not constant and varies strongly for different parameters. It is therefore important to explore how sensitive sub-grid approaches are to DEM uncertainty. To assess this robustness, a DEM uncertainty model (Hebeler and Purves, 2008b) is used to simulate GLOBE DEM error. The GLOBE DEM became available at 30-arcsec resolution in 1998, and was derived from a number of different data sources. Although known to contain a number of flaws and errors, it is still widely being used and currently the only continuous DEM data set available for latitudes above 60°N. Applying the DEM uncertainty model, a suite of 100 uncertainty surfaces are produced at 1 km resolution, where each value represents the potential deviation of elevation at a location.

These surfaces are then added to the original topography and re-sampled to the corresponding target resolutions of 5 and 10 km, delivering a set of 100 different topographies for 1, 5 and 10 km resolution. Using a MCS approach, potential melt is then calculated using the simple TIM at 1 km resolution on each of the 100 surfaces and re-sampled to 5 and 10 km serving as a reference according to Section 2.5. For each 100 surfaces at 5 and 10 km, melt is also calculated using both an unparameterized (baseline) and a sub-grid approach. Finally, the mean and standard deviations of melt for each grid cell across each set of DEMs at the 5 and 10 km resolution are calculated, allowing comparison of the impact of uncertainty on melt variation across the different methods and resolutions.

## RESULTS

#### Basic resolution effects

Comparing the **reference** potential melt across the varying resolutions, it is noticeable that melt ceases to be

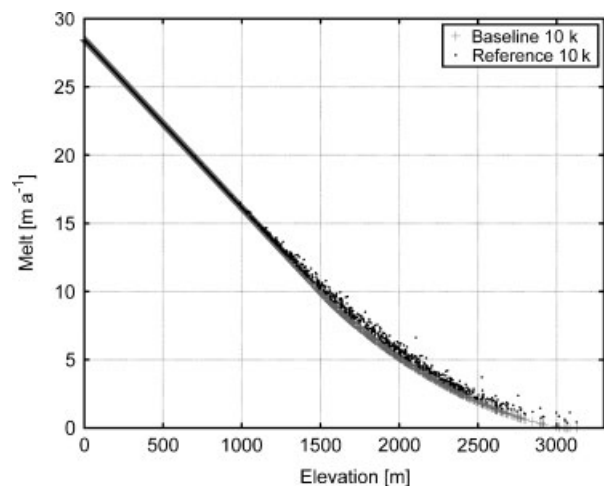


Figure 7. Baseline melt calculated on the 10 km DEM and reference melt averaged from 100 m to 10 km resolution, plotted against elevation

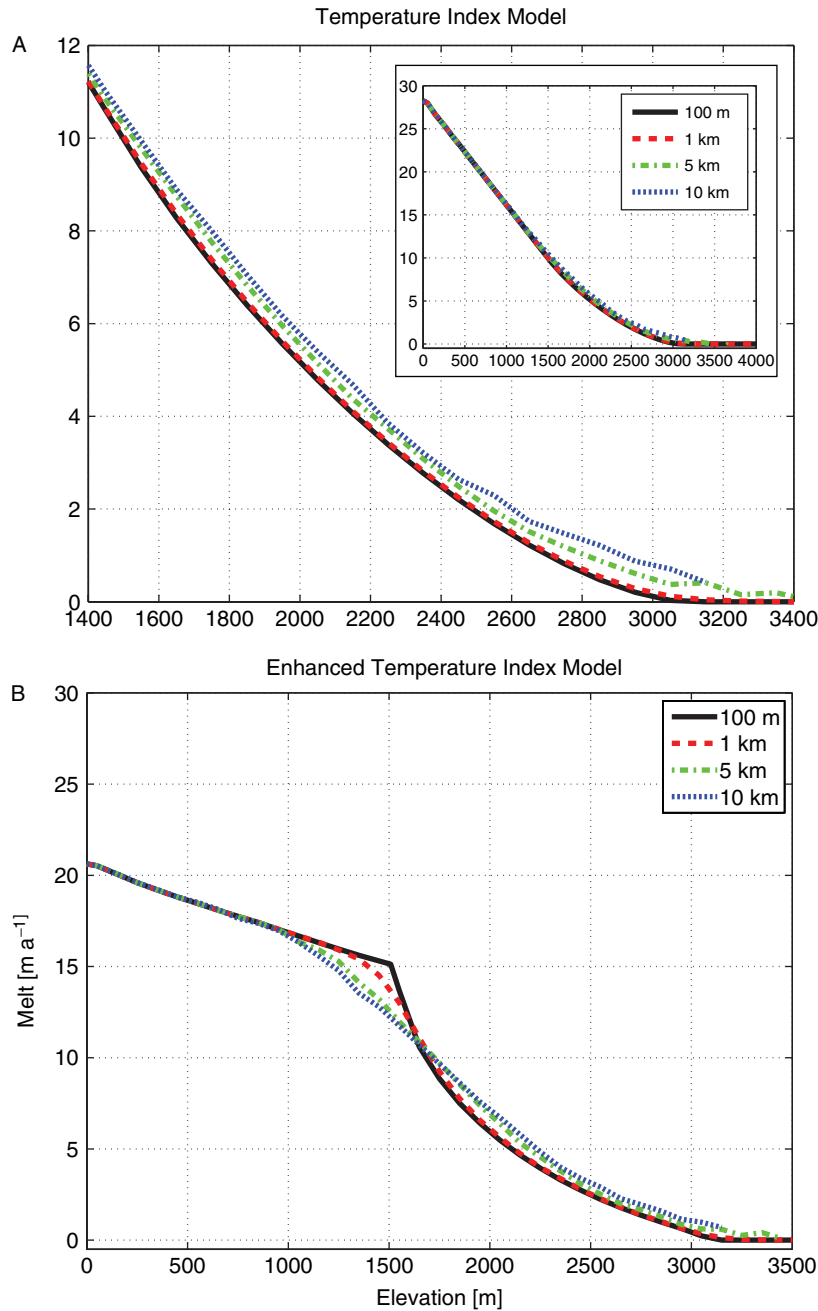


Figure 8. Mean melt versus altitude for the simple TIM (A) and the eTIM(B) for four different resolutions (0.1, 1, 5 and 10 km). For both models, the melt function becomes nonlinear above a threshold at approximately 1500 m at the reference resolution of 100 m. For areas above this threshold, temperatures are below 0°C and melt becomes zero for increasing time spans during the year, and mean melt per altitude increases with decreasing resolution

a simple function of elevation for lower resolutions above a certain threshold elevation. Instead, potential melt can take on a range of values (Figure 7) when plotted against elevation. This effect is triggered by equifinality in the re-sampling: because of the nonlinear dependency of melt on elevation, different hypsometries at the 100 m resolution result in identical mean melt rates. While these identical melt rates are preserved through re-sampling to lower resolutions through averaging, the respective mean elevation values at the low resolution may differ. Hence different elevations at the low resolution can feature the same mean melt rates.

Figure 8A shows the mean melt within 100 m elevation bins range plotted against elevation for the different resolutions. Above a certain elevation threshold (around 1500 m in Figure 8A), for the TIM an increase in melt rates is observable for decreasing resolutions. While the same generally holds for the eTIM, there is a pronounced reduction in mean melt observable for elevations around 1500 m with decreasing resolution (Figure 8B). Compared to the high resolution reference calculated at 100 m, lower resolutions effectively show lower mean melt rates for elevations around 1500 m and higher mean melt rates for elevations above 1700 m.

Table III. Mean melt and RMSE (in brackets) in m w.e. a<sup>-1</sup> for the two approaches (baseline and sub-grid 1) across resolutions of 1, 5 and 10 km, compared to the corresponding reference melt for the TIM. Values are given for the whole of the study area for each resolution, as well as for areas above 1500 m and 2500 m, where temperature drops below 0 °C for increasing time spans during the year

TIM									
Resolution	1 km			5 km			10 km		
	All	≥1500	≥2500	All	≥1500	≥2500	All	≥1500	≥2500
Reference	17.29	4.63	0.93	17.29	5.23	1.33	17.29	5.65	1.69
Baseline	17.28 (0.38)	4.57 (0.74)	0.88 (0.66)	17.18 (0.44)	4.86 (0.84)	1.01 (0.76)	17.11 (0.34)	5.07 (0.64)	1.10 (1.65)
Sub-grid1	17.29 (0.31)	4.62 (0.34)	0.92 (0.20)	17.29 (0.19)	5.14 (0.23)	1.24 (0.02)	17.29 (0.13)	5.50 (0.17)	1.51 (0.20)

Sub-grid approaches

Figure 9A shows a comparison of calculations of potential melt modelled for the reference, baseline and sub-grid 1 approach using the TIM at 10 km resolution. Table III shows mean melt and the associated RMSE for the reference, baseline and sub-grid 1 parameterizations, while Figure 10 shows the spatial distribution of locations with no melt over the entire model region for all resolutions.

The following features are notable:

- Figure 9A shows that the relationship of melt to elevation is broadly similar for all realizations. However, above the LT elevation, Figure 9A clearly illustrates the better performance of the sub-grid 1 approach compared to the baseline.
- Table III shows that sub-grid 1 has lower RMSE values for all resolutions and elevation bands, and thus appears to better approximate the reference melt.
- The baseline and sub-grid 1 RMSE values for the 1 km model are very similar, however a significant improvement in performance is present for elevations above 1500 m and all elevation bands for the 5 and 10 km model runs.
- Areas without melt (Figure 10) are lost due to averaging using the reference approach, while the spatial pattern of melt-free areas is generally preserved using the baseline approach, with the absolute area decreasing by about half between the 1 and 10 km resolutions. Using the sub-grid 1 approach, the total number of cells without any melt (in all sub-grids) decreases with lower resolution, even though it is less pronounced than for the reference approach.

Table IV shows a comparison of three sub-grid parameterization approaches adopted for the eTIM with the baseline and reference potential melt. Since the sub-grid 2 and sub-grid 3 approach are very similar in their results and both have larger RMSEs than the baseline method for all resolutions, these are discarded in further reporting and comparisons are made with only sub-grids 1 and 4. Figure 9B shows the corresponding relationship between elevation and the reference, baseline and sub-grid approaches for the 10 km resolution.

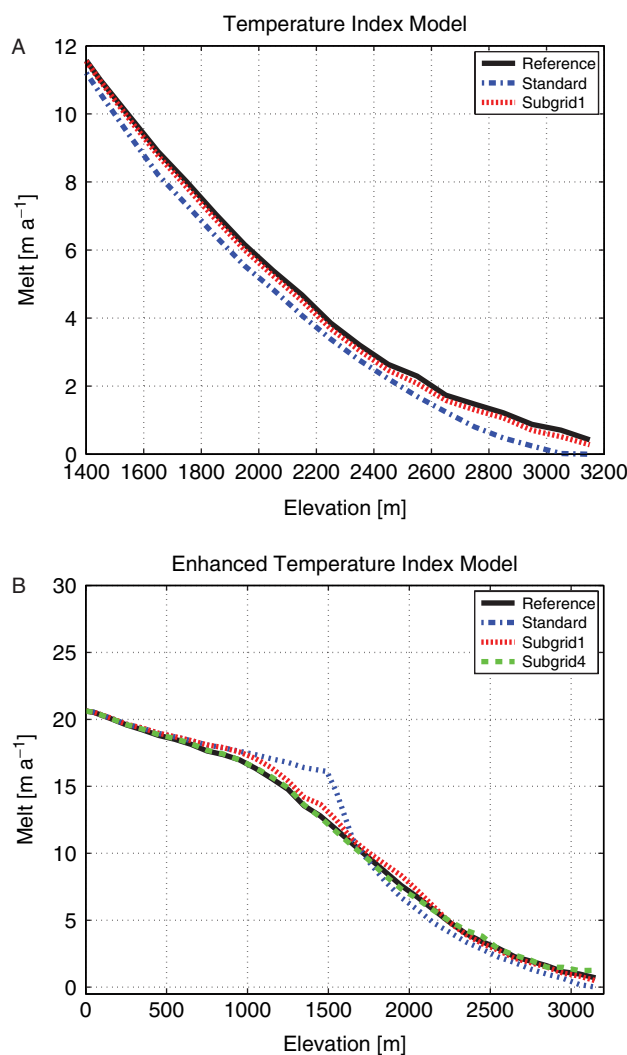


Figure 9. Mean melt versus altitude for different parameterizations of both the TIM (A) and eTIM (B) at 10 km resolution. Elevation ranges are similar to those in Figure 8

- In contrast to the TIM, Figure 9B shows a pronounced difference in melt for elevations between 1000 and 1600 m comparing the baseline with the reference and sub-grid approaches, while above ~1700 m all realizations are broadly similar.
- Table IV shows that sub-grid 1 is clearly an improvement over the baseline approach for all resolutions and

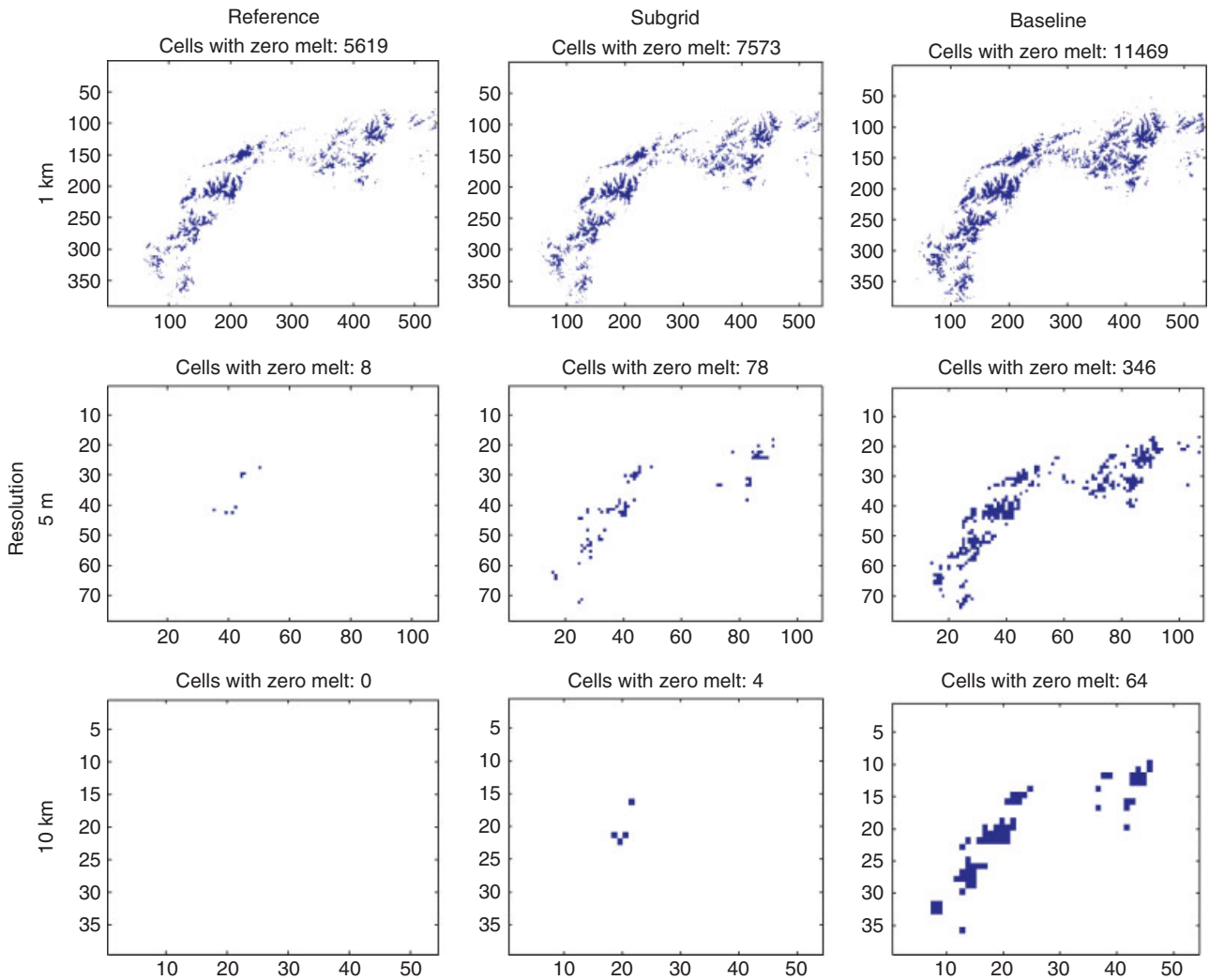


Figure 10. Matrix showing all cells with no melt across the model domain (Figure 2) in blue for the simple TIM. Different resolutions in rows, calculation methods in columns. For the reference melt (left column), the total area without melt decrease with lower resolutions, while the total melt per area is preserved. In the standard approach (right column), the pattern of melt-free cells is preserved. The sub-grid 1 approach (centre column) preserves some of the melt free cells

Table IV. Mean melt and RMSE (in brackets) in m w.e. a<sup>-1</sup> for the four approaches (baseline and Sub-grid 1,2 and 4) across resolutions of 1, 5 and 10 km, compared to the corresponding reference melt for the eTIM. Values are given for the whole of the study area for each resolution, as well as for areas above 1500 m and 2500 m, where temperature drops below 0 °C for increasing time spans during the year. Optimal results feature a small difference in mean potential melt as well as low RMSE

		eTIM								
Resolution		1 km			5 km			10 km		
Model	All	≥1500	≥2500	All	≥1500	≥2500	All	≥1500	≥2500	
Reference	15.27	5.84	1.37	15.27	6.50	1.78	15.27	6.91	2.19	
Baseline	15.45 (0.63)	5.89 (0.70)	1.32 (0.24)	15.59 (0.99)	6.39 (1.11)	1.50 (0.39)	15.63 (1.14)	6.65 (1.23)	1.62 (0.68)	
Sub-grid1	15.45 (0.56)	5.97 (0.58)	1.35 (0.23)	15.56 (0.57)	6.73 (0.59)	1.71 (0.20)	15.58 (0.55)	7.13 (0.52)	2.00 (0.24)	
Sub-grid2	15.27 (0.77)	5.78 (0.87)	1.34 (0.40)	15.29 (1.18)	6.42 (1.45)	1.65 (0.66)	15.30 (1.27)	6.77 (1.56)	1.89 (0.82)	
Sub-grid4	15.29 (1.08)	5.60 (2.07)	3.43 (2.25)	15.28 (0.47)	6.52 (0.89)	2.59 (1.10)	15.29 (0.34)	6.86 (0.61)	2.28 (0.61)	

elevations, with significant improvements for the 5 and 10 km resolutions.

- Sub-grid 2 shows no improvement at any resolution.
- Sub-grid 4 shows the best overall fit with reference melt for the 5 and 10 km resolutions, demonstrated by the

lowest RMSE values (Table IV), but a poor fit at the 1 km resolution.

- While Sub-grid 4 shows the best overall fit for the 5 km resolution, the quality of the fit decreases for higher elevations and overestimates melt for elevations above 2500 m at this resolution.

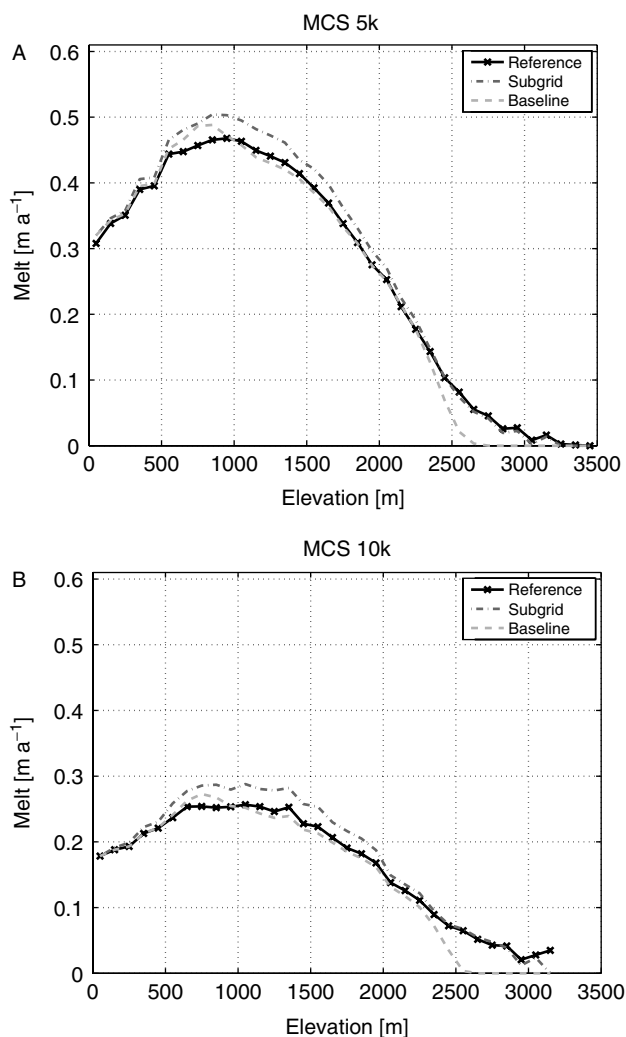


Figure 11. Standard deviation of melt over 100 MCS runs versus elevation bands for the baseline, reference and sub-grid 1 approach for the simple TIM at 5 km (A) and 10 km (B) resolution. The sub-grid approach shows increased susceptibility to DEM uncertainty for elevations below 2000 m, demonstrated by the higher standard deviation. For higher elevations, standard deviations of the sub-grid approach are comparable to the reference. Note that for the baseline approach, no melt is calculated above 2600 m, hence standard deviation becomes zero, while both sub-grid and reference methods show melt rates in the order of 0.5 m/a

#### Uncertainty analysis

Having run the TIM model at 5 and 10 km resolution on 100 topographies perturbed using simulated DEM uncertainty, the mean standard deviation across the 100 runs for elevation classes of 100 m range is plotted against elevation in Figure 11. It is apparent that the standard deviation of melt rates is about 5–10% higher for the sub-grid parameterized approach compared to the baseline for elevations below  $\sim 2000$  m, for both resolutions of 5 and 10 km. Compared to absolute TIM reference melt rates (Figure 8A), the standard deviations amount to around 5% at 5 km resolution, and around 2.5% at 10 km resolutions, for elevations above 2000 m. For areas below 2000 m, the relative standard deviation becomes as low as 1%. For elevations above 2000 m, the standard deviation of the sub-grid 1 parameterization is almost identical

to that of the reference approach. Note that the standard deviation for the baseline approach drops to zero around 2500 m (Figure 9), while both reference and sub-grid 1 values only become zero around 3200 m. This effect is due to the fact that the baseline approach underestimates melt rates, which therefore become zero earlier.

In general, it can be said that melt rates calculated using the TIM at low resolutions show variation of less than 5% when subject to typical GLOBE DEM data uncertainty.

## DISCUSSION

#### Resolution effects

The resolution experiments, averaging the reference melt from 100 m to lower resolutions reveal potential melt to be dependent on terrain roughness (Figure 12). This effect is demonstrated by the scattering of potential melt rates as a function of elevation shown in Figure 7. Cells above the LT elevation will experience temperatures below zero during some interval of the year (described in the Section Method Comparison), which is when melt will become zero (Equations 1 and 3). When aggregated to lower resolution, cells at the 100 m resolution will therefore contribute less to the average melt than cells below LT. The mean melt at a low-resolution cell, averaged from 100 m, is therefore dependent on the number of cells with temperatures below zero during some interval of the year. Additionally, it is influenced by the length of that interval, which is determined by the seasonal temperature variation applied to the MAAT. This temperature variation is a nonlinear (sinusoidal) function, and is the reason for the nonlinear behaviour of the otherwise linear melt function.

Generally, the deviation of mean melt between two resolutions for a given elevation (Figure 8) depends on the amount of scaling, that is the difference in resolutions. The amount a TIM underestimates this reference melt, is dependent on the resolution with which it has originally been parameterized and the lower 'target' resolution.

While the origin resolution (in our case the reference at 100 m) should be adequately chosen to capture the scale of the parameterized model processes in order to ascertain sensible comparison of results (Martin and Church, 2004), the target resolution is usually determined by the computational demands of the model or the limitations associated with the input data. In the case of the simple TIM, the origin resolution should thus retain the hypsometry of a topography with minimal possible smoothing. Furthermore, the underestimation of melt will depend on the applied MAAT, lapse rate, and topographic properties such as overall elevation range and roughness, as MAAT and lapse rate control the elevation of the LT and UT.

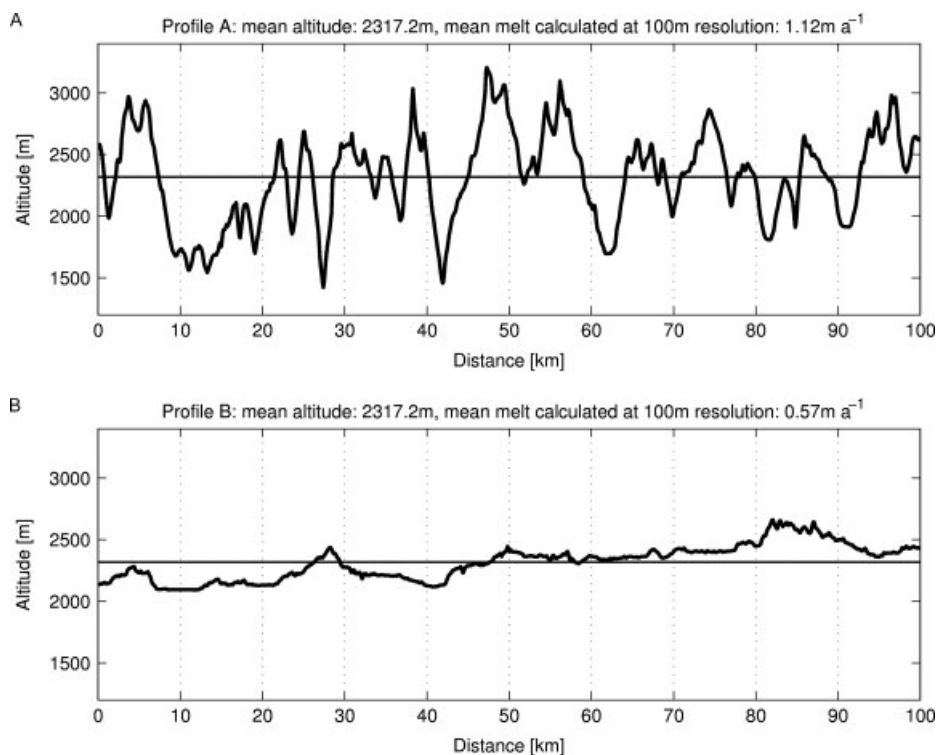


Figure 12. A 100 km profile of the central alps (A), with a mean elevation of 2317.2 m and an elevation range of more than 1500 m. Mean melt calculated for this profile using the TIM is 1.12 m/a. A much smoother profile taken from the South German midlands (B) with an elevation range of just above 600 m was raised to the same mean elevation. Because of the dependence of melt on terrain roughness, the mean potential melt rate calculated is only about half that of profile A at 0.57 m/a

For the eTIM, the effect scaling has on calculation of potential melt is more complex. The sharp transition at the  $0^{\circ}\text{C}$  threshold at the 100 m reference resolution is gradually smoothed with decreasing resolution (Figure 8B). Using the baseline eTIM approach at low resolutions thus results in an overestimation of melt around the lower temperature threshold ( $\sim 1500$  m), which can be as much as 20% at a resolution of 10 km (Figure 8B). Simultaneously, an underestimation of melt for elevations above the threshold, similar to that encountered for the TIM can be observed. As for the TIM, a suitable reference resolution (origin) needs to retain topographic features that are important to characterizing the process of interest (Martin and Church, 2004). In the case of the eTIM this is elevation and the average slope length, which is necessary to capture the spatial variation of slope and aspect, used to calculate radiation based melt. For both the TIM and eTIM, the resolution of 1 km apparently captures the DEM properties of interest well, as the differences in melt compared to the 100 m resolution are small. The effect of averaging to 5 and 10 km resolution on topographic properties is much larger and reflected in the resulting deviation of melt rates.

#### Method comparison

*TIM modelling approaches.* Even though a simple underestimation of melt in the baseline TIM approach could easily be compensated by adapting the model parameters—for example DDF or temperature—this would require that the melt model was run at a higher

resolution first in order to determine the optimal parameterization. However, looking at the pattern of melt-free cells modelled using the TIM (Figure 10), the dilemma of modelling melt at low resolutions becomes apparent: while the baseline approach retains the spatial pattern, thus keeping the overall area of melt-free cells approximately constant across resolutions, melt rates in these cells underestimate those rates derived at higher resolutions. A simple increase in melt at lower resolutions to fit the reference rates would again result in a loss of melt-free areas. These areas are important, for example, when modelling ice sheet inception or glaciers as global runoff reservoirs, as it has been shown that even a small under- or overestimation of glacierized areas can have a significant influence on run-off regimes (Jansson *et al.*, 2003; Kaser *et al.*, 2003). The problem can be overcome by using the simple sub-grid 1 approach adopted in this article: while the sub-grid 1 parameterization produces melt rates close to the reference (Figure 9), it retains only few cells without any melt (Figure 10). However, the additional elevation information provided by the sub-grids can be included in modelling processes like inception (e.g. Marshall, 2002).

*eTIM modelling approaches.* Comparing the performance of the different sub-grid approaches applied to the eTIM (see Section on Sub-grid Parameterization), the performance of the simple sub-grid 1 parameterization is initially surprising (Table IV). The calculation of slope and aspect on the respective elevation sub-grids is somewhat arbitrary, and one would expect a better fit using

averages from the high-resolution DEM (used in sub-grid 2 and 3). Looking at the dependencies of radiation melt on aspect and slope helps to explain the relatively good performance of the simple sub-grid 1 approach. Aspect has a strong influence on radiation melt (Figure 5), and the re-sampling of aspect to lower resolutions is difficult, as replacing a range of aspects at high resolution with just one value at a lower resolution will inevitably bias any result thus calculated. For the relatively low mean slopes in the range of 0.2–0.3 radians calculated for the sub-grid 1 approach, the resulting deviation in melt for different aspects is small, while high slopes in the range of 0.6–0.7 radians result in a much higher deviation, for example between south and north facing slopes. Averaged across all aspect values, a lower slope generally results in a higher mean melt for our experimental setup. This explains the slight overestimation of melt rates of the sub-grid 1 approach for elevations below 2000 m for the eTIM (Figure 9B), contrary to the slight underestimation of the sub-grid 1 approach for the TIM (Figure 9A).

The sub-grid 4 approach, using sub-grids for the four cardinal directions, performs well across the whole elevation range, with some overestimation of melt at higher elevations. However, while the approach proves to be effective for the 5 and 10 km resolutions, it is not valid for parameterization at the 1 km resolution (Table IV). This might be explained by the fact that average slope length is still captured well at the 1 km resolution, and thus pronounced elevation features, for example slopes predominantly facing one direction, are not averaged out at this scale. Thus, very distinct melt patterns can exist, which are not captured well enough at 1 km using our parameterization, leading to noticeable over- and underestimations for extreme cases. Additionally, while the sub-grid 4 approach shows the best overall fit at 5 km resolution, for elevations above 2500 m calculated potential melt considerably overestimates reference melt, and the approach provides no improvement over the baseline. However, this overestimation is likely to be due to the use of regression parameters for reduction of the radiation melt from the 10 km resolution. While this guarantees an optimal fit for all elevations at this resolution for the sub-grid 4 approach, results are sub-optimal for lower resolutions. While in general, the parameterization concept using directional sub-grids works well, the criteria (Section 1.3) of scalability is not completely fulfilled, and further investigation of the causes and the range of application scales, as well as a possible improvement of the method will be useful.

#### *Uncertainty analysis*

The sub-grid 1 approach shows a slightly increased susceptibility to DEM uncertainty, judged by the standard deviation of melt rates as a function of elevation (Figure 11), than the baseline or reference approaches. This can be explained by the fact that uncertainty introduced to the DEM has a threefold impact on the sub-grid approach, because elevation uncertainty affects all three

sub-grid elevation values via the change of hypsometry. For the reference approach, the DEM uncertainty effects are more likely to be cancelled out over an area of 5 or 10 km. The same holds for the baseline approach, where uncertainties at the higher resolution are also averaged out. This increase in uncertainty of the sub-grid 1 parameterization relative to the reference and baseline approaches is at a maximum 10% for elevations below 2000 m. Because potential melt at these elevations plays a minor role in ablation calculations, this increased uncertainty is probably of little relevance. However, it is important to be aware of the effects of DEM uncertainty when using sub-grid approaches.

#### CONCLUSION

A parameterization using three hypsometric sub-grids has proven to be a simple, robust and scalable method for melt calculation at low resolutions using both simple and eTIMs. The use of sub-grids also provides additional information derived from higher resolution topographies, which can be used in a variety of modelling approaches, from simple masking to complex internal coupling, e.g. as in hydrological modelling across elevation bands.

The parameterization developed for the enhanced solar radiation model, using slope sub-grids for the cardinal directions, proved to provide the best modelling results for resolutions below 5 km, providing very good estimates of higher resolution reference melt rates, if regression parameters for adjusting radiation melt for temperature reduction are derived for each resolution. Performance is decreased if global regression parameters are used that have been derived for a range of resolutions, and the approach is therefore not fully scalable. Further experiments need to assess the threshold resolution for this parameterization approach, as well as the exact reasons for the existence of this threshold. Optimization of regression parameters for the reduction of radiation melt is also needed.

Our experiments using a DEM uncertainty model to test sensitivity of a simple TIM confirm that sub-grid parameterization can be used for modelling sub-scale processes, but care has to be taken when this form of parameterization is applied. Sensitivity studies should be conducted to assure the reliability of the model results is preserved.

#### ACKNOWLEDGEMENTS

This research was funded by the Swiss National Science Foundation SNF, project number 200020-109449. The comments of Dr Gwenn Flowers and the two anonymous reviewers greatly improved this article.

#### REFERENCES

- Albani M, Klinkenberg B, Andison DW, Kimmins JP. 2004. The choice of window size in approximating topographic surfaces from digital

- elevation models. *International Journal of Geographical Information Science* **18**(6): 557–593.
- Alley RB, Clark PU, Huybrechts P, Joughin I. 2005. Ice-sheet and sea-level changes. *Science* **310**: 456–460.
- Armstrong RN, Martz LW. 2003. Topographic parameterization in continental hydrology: a study in scale. *Hydrological Processes* **17**(18): 3763–3781.
- Braithwaite R. 1995. Positive degree-day factors for ablation on the Greenland ice sheet studied by energy-balance modelling. *Journal of Glaciology* **41**(137): 153–159.
- Cazorzi F, Fontana GD. 1996. Snowmelt modelling by combining air temperature and a distributed radiation index. *Journal of Hydrology* **181**: 169–187.
- Endreny TA, Wood EF. 2001. Representing elevation uncertainty in runoff modelling and flowpath mapping. *Hydrological Processes* **15**(12): 2223–2236.
- Essery R, Etchevers P. 2004. Parameter sensitivity in simulations of snowmelt. *Journal of Geophysical Research* **109**: D20111.
- Essery R, Marks D. 2007. Scaling and parametrization of clear-sky solar radiation over complex topography. *Journal of Geophysical Research* **112**: D10122.
- Florinsky IV. 1998. Accuracy of local topographic variables derived from digital elevation models. *International Journal of Geographical Information Science* **12**(1): 47–61.
- Hagdorn M, Rutt I, Payne T, Hebel F. 2006. GLIMMER - The GENIE Land Ice Model with Multiply Enabled Regions - Documentation. <http://glimmer.forge.nesc.ac.uk/>, Universities of Bristol, Edinburgh, Zurich.
- Hastings DA, Dunbar PK. 1998. Development and assessment of the Global Land One-km Base Elevation Digital Elevation Model (GLOBE). *ISPRS Archives* **32**(4): 218–221.
- Hebel F, Purves RS. 2008a. The influence of elevation uncertainty on derivation of topographic indices. *Geomorphology* (in press).
- Hebel F, Purves RS. 2008b. *Modelling DEM Data Uncertainties for Monte Carlo Simulations of Ice Sheet Models*. CRC press: (in press).
- Hock R. 1999. A distributed temperature-index ice- and snowmelt model including potential direct solar radiation. *Journal of Glaciology* **45**(149): 101–111.
- Hock R. 2003. Temperature index melt modelling in mountain areas. *Journal of Hydrology* **282**: 104–115.
- Hock R. 2005. Glacier melt: a review of processes and their modelling. *Progress in Physical Geography* **29**(3): 362–391.
- Hu Z, Islam S. 1997. Effects of spatial variability on the scaling of land surface parameterizations. *Boundary-Layer Meteorology* **83**: 441–461.
- Huybrechts P, Letréguilly A, Reeh N. 1991. The Greenland ice sheet and greenhouse warming. *Global and Planetary Change* **3**(4): 399–412.
- Huybrechts P, Payne A, Abe-Ouchi A, Calov R, Fabre A, Fastook J, Greve R, Hindmarsh R, Hoydal O, Jóhannesson T. 1996. The EISMINT benchmarks for testing ice-sheet models. *Annals of Glaciology* **23**: 1–12.
- Jansson P, Hock R, Schneider T. 2003. The concept of glacier storage: a review. *Journal of Hydrology* **282**: 116–129.
- Jarvis A, Reuter H, Nelson A, Guevara E. 2006. Void-filled seamless SRTM data V3, available from the CGIAR-CSI SRTM 90m Database, <http://srtm.csi.cgiar.org>, International Centre for Tropical Agriculture (CIAT).
- Kaser G, Juen I, Georges C, Gómez J, Tamayo W. 2003. The impact of glaciers on the runoff and the reconstruction of mass balance history from hydrological data in the tropical Cordillera Blanca, Perú. *Journal of Hydrology* **282**: 130–144.
- Kumar L, Skidmore AK, Knowles E. 1997. Modelling topographic variation in solar radiation in a GIS environment. *International Journal of Geographical Information Science* **11**: 475–497.
- Lefebvre F, Gallée H, van Ypersele J-P, Greuell W. 2003. Modeling of snow and ice melt at ETH camp (West Greenland): a study of surface albedo. *Journal of Geophysical Research* **108**(D8): 4231.
- Leung LR, Wigmosta MS, Ghan SJ, Epstein DJ, Vail LW. 1996. Application of a subgrid orographic precipitation/surface hydrology scheme to a mountain watershed. *Journal of Geophysical Research* **101**(D8): 12 803–12 818.
- Luce CH, Tarboton DG, Cooley KR. 1999. Sub-grid parameterization of snow distribution for an energy and mass balance snow cover model. *Hydrological Processes* **13**: 1921–1933.
- Malanson GP. 1999. Considering complexity. *Annals of the Association of American Geographers* **89**(4): 746–753.
- Marshall SJ. 2002. Modelled nucleation centres of the Pleistocene ice sheets from an ice sheet model with subgrid topographic and glaciologic parameterizations. *Quaternary International* **95–96**: 125–137.
- Marshall SJ, Clarke G. 1999. Ice sheet inception: subgrid hypsometric parameterization of mass balance in an ice sheet model. *Climate Dynamics* **15**: 533–560.
- Martin Y, Church M. 2004. Numerical modelling of landscape evolution: geomorphological perspectives. *Progress in Physical Geography* **28**(3): 317–339.
- Oksanen J, Sarjakoski T. 2005. Error propagation of DEM-based surface derivatives. *Computers & Geosciences* **31**(8): 1015–1027.
- Pellicciotti F, Brock B, Strasser U, Burlando P, Funk M, Corripio J. 2005. An enhanced temperature-index glacier melt model including the shortwave radiation balance: development and testing for Haut Glacier d'Arolla, Switzerland. *Journal of Glaciology* **51**(175): 573–587.
- Ritz K, Fabre A, Letréguilly A. 1997. Sensitivity of a Greenland ice sheet model to ice flow and ablation parameters: consequences for the evolution through the last climatic cycle. *Climate Dynamics* **13**(1): 11–24.
- Salzmann N, Frei C, Vidale P-L, Hoelzle M. 2007. The application of regional climate model output for the simulation of high-mountain permafrost scenarios. *Global and Planetary Change* **56**: 188–202.
- Schneeberger C, Blatter H, Abe-Ouchi A, Wild M. 2003. Modelling changes in the mass balance of glaciers of the northern hemisphere for a transient 2× CO<sub>2</sub> scenario. *Journal of Hydrology* **282**: 145–163.
- Stone PH, Carlson JH. 1979. Atmospheric lapse rate regimes and their parameterization. *Journal of Atmospheric Sciences* **3**: 415–423.
- Strasser U, Etchevers P. 2003. Using subgrid parameterization for topography and a forest canopy climate model for improving snowmelt flood simulations. In *Climatology and Hydrology of Mountain Areas*, de Jong C, Collins D, Ranzi R (eds). John Wiley and Sons Chichester.
- Strasser U, Corripio J, Pellicciotti F, Burlando P. 2004. Spatial and temporal variability of meteorological variables at Haut Glacier d'Arolla (Switzerland) during the ablation season 2001: Measurements and simulations. *Journal of Geophysical Research* **109**: D03103.
- Wechsler SP. 2000. Effect of DEM uncertainty on topographic parameters, DEM scale and terrain evaluation, Dissertation, State University of New York, College of Environmental Science and Forestry, Syracuse.
- Wechsler SP. 2007. Uncertainties associated with digital elevation models for hydrologic applications: a review. *Hydrology and Earth System Sciences* **11**(4): 1481–1500.
- Williams KS, Tarboton DG. 1999. The ABC's of snowmelt: a topographically factorized energy component snowmelt model. *Hydrological Processes* **13**: 1905–1920.
- Zhang X, Drake NA, Wainwright J, Mulligan M. 1999. Comparison of slope estimates from low resolution DEMs: scaling issues and a fractal method for their solution. *Earth Surface Processes and Landforms* **24**(9): 763–779.